Fusion Engineering and Design 146 (2019) 555–558

Contents lists available at ScienceDirect

Fusion Engineering and Design

journal homepage: www.elsevier.com/locate/fusengdes

TRANSP-based closed-loop simulations of current profile optimal regulation in NSTX-Upgrade

Zeki O. Ilhan[a,*], Mark D. Boyer[b], Eugenio Schuster[a]

[a] Department of Mechanical Engineering and Mechanics, Lehigh University, Bethlehem, PA 18015, USA
[b] Princeton Plasma Physics Laboratory, Princeton, NJ 08540, USA

ARTICLE INFO

Keywords:
Plasma control
Current profile control
Model-based control
Optimal control
TRANSP-based simulation

ABSTRACT

Active control of the toroidal current density profile is critical for the upgraded National Spherical Torus eXperiment device (NSTX-U) to maintain operation at the desired high-performance, MHD-stable, plasma regime. Initial efforts towards current density profile control have led to the development of a control-oriented, physics-based, plasma-response model, which combines the magnetic diffusion equation with empirical correlations for the kinetic profiles and the non-inductive current sources. The developed control-oriented model has been successfully tailored to the NSTX-U geometry and actuators. Moreover, a series of efforts have been made towards the design of model-based controllers, including a linear-quadratic-integral optimal control strategy that can regulate the current density profile around a prescribed target profile while rejecting disturbances. In this work, the tracking performance of the proposed current-profile optimal controller is tested in numerical simulations based on the physics-oriented code TRANSP. These high-fidelity closed-loop simulations, which are a critical step before experimental implementation and testing, are enabled by a flexible framework recently developed to perform feedback control design and simulation in TRANSP.

1. Introduction

The National Spherical Torus eXperiment-Upgrade (NSTX-U) [1] is located in Princeton Plasma Physics Laboratory (PPPL) in the USA. Compared to the former NSTX device, it has significantly higher toroidal field and solenoid capabilities, and three additional neutral beam sources with significantly larger current-drive efficiency [2]. The main mission of the NSTX-U research program is to establish the physics basis for the compact spherical tokamak (ST) as a candidate for a Fusion Nuclear Science Facility (FNSF), which is a critical major next step in the US fusion program [3]. At the same time, the unique operating regimes of NSTX-U can contribute to several important issues in the physics of burning plasmas to optimize the performance of ITER [3].

Having the capability of consistently setting up a suitable current density profile is a key step towards achieving the desired advanced-tokamak operating regime in NSTX-U, which is characterized by the non-inductive sustainment of high-β, high-performance, equilibrium scenarios with neutral beam heating and longer pulse durations [2]. As a first step towards active current-profile control in NSTX-U, a so-called first-principles-driven (FPD) plasma response model has been proposed by combining a first-principles equation like the magnetic diffusion equation with empirical correlations for the electron density, electron temperature, plasma resistivity, and non-inductive current sources [4]. After tailoring the proposed FPD model to the NSTX-U geometry and actuators, it is incorporated into the control design process to produce a linear-quadratic-integral optimal controller that can track a prescribed current-profile target while dealing with model uncertainties and rejecting external disturbances. In addition to electron density and total plasma current, which are in turn regulated by dedicated controllers, auxiliary heating/current-drive sources (i.e., the six neutral beam injectors available after the upgrade) are used as actuators to shape the current profile in NSTX-U.

Due to the highly complex physical behavior of tokamak plasmas, controllers tested in simulations based on control-oriented models might fail to satisfy the desired performance criteria when directly tested on the real device. For this reason, a more physics-oriented simulation stage is proposed in this work before actually implementing the controller in NSTX-U. Therefore, the effectiveness of the proposed controller in regulating the current profile in NSTX-U is demonstrated through closed-loop nonlinear simulations based on the high-fidelity physics-oriented code, TRANSP [5], using the recently developed flexible framework for control testing [6].

* Corresponding author.
E-mail address: ilhan@alum.lehigh.edu (Z.O. Ilhan).

https://doi.org/10.1016/j.fusengdes.2019.01.021
Received 4 October 2018; Received in revised form 21 December 2018; Accepted 4 January 2019
Available online 19 February 2019

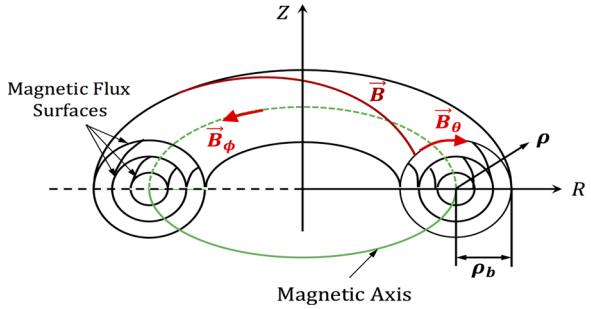

Fig. 1. Magnetic flux surfaces in a tokamak. The helical magnetic field ($\vec{B}$) in a tokamak plasma is composed of toroidal ($\vec{B}_\phi$) and poloidal ($\vec{B}_\theta$) fields.

2. Rotational transform profile evolution model

In a tokamak plasma, points of constant magnetic flux form nested concentric surfaces as depicted in Fig. 1. In principle, magnetic flux surfaces can be associated with any quantity that stays constant on these surfaces. It is convenient to choose the mean effective minor radius of the flux surfaces as an index variable, as it relates to the toroidal magnetic flux Φ as $\Phi = \pi B_{\phi,0}\rho^2$, where $B_{\phi,0}$ is the toroidal magnetic field at the geometric major radius R_0 of the tokamak. To make this index variable non-dimensional, the normalized mean effective minor radius can be defined as $\hat{\rho} = \rho/\rho_b$, where ρ_b is the mean effective minor radius of the last closed flux surface as shown in Fig. 1.

The toroidal current density in the tokamak can be written as

$$j_\phi(\hat{\rho}, t) = -\frac{1}{\mu_0 \rho_b^2 R_0 \hat{H}} \frac{1}{\hat{\rho}} \frac{\partial}{\partial \hat{\rho}} \left(\hat{\rho} \hat{G} \hat{H} \frac{\partial \psi}{\partial \hat{\rho}} \right), \tag{1}$$

where μ_0 is the permeability of the free space, $\hat{G}$, $\hat{H}$ are geometrical factors associated with the plasma equilibrium, and ψ is the poloidal stream function, which is related to the poloidal magnetic flux Ψ as $\Psi = 2\pi\psi$ [7]. The rotational transform ι, which is the inverse of the safety factor q, is further related to the poloidal stream function gradient profile, $\partial\psi/\partial\hat{\rho}$, as

$$\iota(\hat{\rho}, t) = -\frac{d\Psi}{d\Phi} = -\frac{\partial\psi/\partial\hat{\rho}}{B_{\phi,0}\rho_b^2\hat{\rho}}. \tag{2}$$

It is evident from (1) and (2) that the toroidal current density (j_ϕ), rotational transform (ι), and poloidal flux (Ψ) could be used interchangeably for current-profile control design.

The control-oriented partial-differential-equation (PDE),

$$\frac{\partial \psi}{\partial t} = f_\eta u_\eta \frac{1}{\hat{\rho}} \frac{\partial}{\partial \hat{\rho}} \left(\hat{\rho} D_\psi \frac{\partial \psi}{\partial \hat{\rho}} \right) + \sum_{i=1}^{6} f_i u_i + f_{\text{bs}} u_{\text{bs}} \left(\frac{\partial \psi}{\partial \hat{\rho}} \right)^{-1}, \tag{3}$$

with boundary conditions $\partial\psi/\partial\hat{\rho}|_{\hat{\rho}=0} = 0$, $\partial\psi/\partial\hat{\rho}|_{\hat{\rho}=1} = -k_{I_p} u_{I_p}$, has been proposed to model the evolution of the ψ profile [4] as a control-oriented version of the magnetic diffusion equation (MDE). The spatial functions D_ψ, f_η, f_i, f_{bs}, and k_{I_p} can be expressed in terms of the various reference profiles and constants used in the scenario-specific, equilibrium-dependent, control-oriented models developed for the electron density and temperature profiles, the noninductive current sources, and the plasma resistivity in NSTX-U [4]. The model used for control synthesis makes the simplifying assumption that the magnetic geometry is fixed in time, which makes these spatial functions constant over time. Eq. (3) admits diffusivity (u_η), interior (u_i, u_{bs}) and boundary (u_{I_p}) control terms, where each of them represents nonlinear combinations of the physical actuators, $u = [\bar{n}_e, P_1, P_2, P_3, P_4, P_5, P_6, I_p] \in \mathbb{R}^{8\times 1}$, and can be defined as $u_\eta(t) = u_n(t)^{3/2} I_p(t)^{-3/2} P_{tot}(t)^{-3/4}$, $u_i(t) = P_i(t) I_p(t)^{-1} P_{tot}(t)^{-1/2}$, $u_{bs}(t) = u_n(t)^{3/2} I_p(t)^{-1/2} P_{tot}(t)^{-1/4}$, and $u_{I_p}(t) = I_p(t)$, where I_p is the total plasma current, P_i is the individual neutral beam injector powers ($i = 1, \ldots, 6$), $P_{\text{tot}}(t) = \sum_{i=1}^{6} P_i(t)$, $\bar{n}_e$ is the line-averaged electron density, and $u_n = \bar{n}_e/\bar{n}_e^{\text{ref}}$, where $\bar{n}_e^{\text{ref}}$ is the reference profile used in the simplified model for the line-averaged electron density [4].

As the rotational transform ι depends on the poloidal magnetic flux gradient profile, we define $\theta(\hat{\rho}, t) \triangleq \partial\psi/\partial\hat{\rho}$, and by differentiating (3) with respect to $\hat{\rho}$, the PDE governing the evolution of $\theta(\hat{\rho}, t)$ can be written as

$$\frac{\partial \theta}{\partial t} = u_\eta (h_0 \theta'' + h_1 \theta' + h_2 \theta) + \frac{u_{\text{bs}}}{\theta} \left(f'_{\text{bs}} - f_{\text{bs}} \frac{\theta'}{\theta} \right) + \sum_{i=1}^{6} f'_i u_i, \tag{4}$$

with boundary conditions $\theta|_{\hat{\rho}=0} = 0$, $\theta|_{\hat{\rho}=1} = -k_{I_p} u_{I_p}$, where $(\cdot)' = \partial/\partial\hat{\rho}$ for simplicity, and the spatial functions h_0, h_1, h_2 are written as $h_0 = D_\psi f_\eta$, $h_1 = \left(D'_\psi + \frac{1}{\hat{\rho}} D_\psi + D'_\psi\right) f_\eta + D_\psi f'_\eta$, and $h_2 = \left(D''_\psi + \frac{1}{\hat{\rho}} D'_\psi - \frac{1}{\hat{\rho}^2} D_\psi\right) f_\eta + \left(D'_\psi + \frac{1}{\hat{\rho}} D_\psi\right) f'_\eta$.

2.1. Model reduction via spatial discretization

To facilitate control design, the governing PDE (4) is discretized in space, leaving the time domain continuous. The non-dimensional spatial domain $\hat{\rho} \in [0,\ 1]$ is divided into l nodes, hence, the radial grid size becomes $\Delta\hat{\rho} = 1/(l-1)$. After applying the finite difference approximations to the spatial derivatives, the discrete form of (4) yields a set of nonlinear ODEs

$$\dot{\theta} = g(\theta, u), \tag{5}$$

where $\theta = [\theta_2, \theta_3, \ldots, \theta_n]^T \in \mathbb{R}^{n\times 1}$ is the state vector ($n = l - 2$), θ_i is the discrete values of the θ-profile at each inner node, $u \in \mathbb{R}^{8\times 1}$ is the already defined vector of physical actuators, $g \in \mathbb{R}^{n\times 1}$ is a nonlinear function of the system inputs and states.

2.2. Model linearization

Let $u_r(t)$ and $\theta_r(t)$ define a set of reference trajectories for the physical actuators and the system states satisfying the nonlinear, reduced-order model (5), i.e.,

$$\dot{\theta}_r = g(\theta_r, u_r). \tag{6}$$

A model suitable for tracking control design can be obtained by defining the perturbation variables $\Delta\theta(t) = \theta(t) - \theta_r(t)$ and $\Delta u(t) = u(t) - u_r(t)$, where $\Delta\theta(t)$ is the deviation away from the reference state trajectory and $\Delta u(t)$ is the to-be-designed feedback control law. By using (6) and a first-order Taylor series expansion of g in (5) around θ_r and u_r, it is possible to obtain the approximate linear time-variant (LTV) model

$$\Delta\dot{\theta}(t) \approx \frac{\partial g}{\partial \theta}|_{\theta_r(t), u_r(t)} \Delta\theta(t) + \frac{\partial g}{\partial u}|_{\theta_r(t), u_r(t)} \Delta u(t), \tag{7}$$

where $\partial g/\partial\theta \in \mathbb{R}^{n\times n}$ and $\partial g/\partial u \in \mathbb{R}^{n\times 8}$ are the system Jacobians. After the initial ramp-up phase of the plasma discharge, u_r and θ_r remain approximately constant, and as an additional approximation the Jacobians can be evaluated at a specific time t_s to obtain the linear time-invariant (LTI) model given by

$$\Delta\dot{\theta}(t) \approx A\Delta\theta(t) + B\Delta u(t), \quad y(t) = C\Delta\theta(t), \tag{8}$$

where $A = (\partial g/\partial\theta)|_{\theta_r(t_s), u_r(t_s)}$, $B = (\partial g/\partial u)|_{\theta_r(t_s), u_r(t_s)}$, t_s is some time during the flat-top phase of the discharge, $C \in \mathbb{R}^{m\times n}$ is the output matrix, and $y(t) \in \mathbb{R}^{m\times 1}$ is the output vector with $m = 8$ (number of control outputs chosen equal to the number of available physical actuators). Using (2), the LTI model (8) for $\Delta\theta$ can be converted into an LTI model for $\Delta\iota$ as

$$\Delta\dot{\iota}(t) \approx \bar{A}\Delta\iota(t) + \bar{B}\Delta u(t), \quad y(t) = \bar{C}\Delta\iota(t), \tag{9}$$

where $\bar{A} = T^{-1}AT$, $\bar{B} = T^{-1}B$, $\bar{C} = TC$, with the transformation matrix $T = -\text{diag}(B_0\rho_b^2\hat{\rho}_i)$, where $\hat{\rho}_i = i(\Delta\hat{\rho})$, for $i = 1, 2, \ldots, n$.

3. Optimal control design

Let $\iota_r(t)$ represent a target rotational transform profile to achieve. The tracking problem for $\iota(t)$ then becomes a regulation problem for $\Delta\iota(t)$, since $\Delta\iota(t) = \iota(t) - \iota_r(t)$. Therefore, the control objective is to regulate the output $y(t)$ around zero with minimum control effort. To improve upon the tracking performance and disturbance rejection, integral action should be added to the standard optimal control solution, leading to a linear-quadratic-integral (LQI) control design.

To obtain the LQI controller, an enlarged state variable $\tilde{x}(t)$ can be introduced by augmenting the actual state $\Delta\iota(t)$ with the time integral of the output vector

$$\tilde{x}(t) = \begin{bmatrix} \int_0^t y(\tau)\,d\tau \\ \Delta\iota(t) \end{bmatrix} = \begin{bmatrix} \int_0^t \bar{C}\Delta\iota(\tau)d\tau \\ \Delta\iota(t) \end{bmatrix}. \tag{10}$$

Taking the time derivative of (10) and using (9), a new, augmented system can be obtained as

$$\dot{\tilde{x}}(t) \approx \tilde{A}\tilde{x}(t) + \tilde{B}\Delta u(t), \tag{11}$$

where $\tilde{A} = \begin{bmatrix} 0 & \bar{C} \\ 0 & \bar{A} \end{bmatrix}$ and $\tilde{B} = \begin{bmatrix} 0 \\ \bar{B} \end{bmatrix}$. The optimal control problem can then be stated in terms of the enlarged system (11) as

$$\min_{\Delta u(t)} J = \frac{1}{2}\int_{t_0}^{\infty} [\tilde{x}^T Q\tilde{x} + \Delta u^T R\Delta u]\,\mathrm{d}t, \tag{12}$$

where $Q \in \mathbb{R}^{(m+n)\times(m+n)}$, and $R \in \mathbb{R}^{m\times m}$ are symmetric, positive definite weight matrices. The optimal control law is given by

$$\Delta u(t) = -K\tilde{x}(t), \tag{13}$$

where $K = R^{-1}\tilde{B}^T P_+$, and P_+ is the unique positive definite solution to the Algebraic Riccati Equation [8]

$$0 = -\tilde{A}^T P_+ - P_+\tilde{A} + P_+\tilde{B}R^{-1}\tilde{B}^T P_+ - Q. \tag{14}$$

Finally, using (10) for $\tilde{x}$, the optimal control law (13) becomes

$$\Delta u(t) = -K_I \int_{t_0}^{t} \bar{C}\Delta\iota(\tau)d\tau - K_P\Delta\iota(t), \tag{15}$$

where $K_I \in \mathbb{R}^{m\times m}$ and $K_P \in \mathbb{R}^{m\times n}$ are the partitions of the optimal gain K, i.e., $K = [K_I\ K_P]$. Note that the optimal solution (15) yields a PI (Proportional plus Integral) control law.

4. Closed-loop TRANSP simulation results

The necessary modifications to enable feedback control simulations in TRANSP have been implemented through the so-called Expert routine [6]. It interrupts the standard operation of the TRANSP code at each time step to recalculate the actuator requests according to the implemented feedback control law and the current plasma state.

At the beginning of each TRANSP transport time step, the Expert routine is called and it performs the necessary modifications through its four main modules (Fig. 2). The electron density module supplies an electron density profile to the TRANSP by scaling an experimental electron density profile shape (n_e^{ref}) to achieve a target line-averaged density, $\bar{n}_e(t)$. Similarly, the electron temperature module supplies an electron temperature profile to the TRANSP by scaling an experimental profile to maintain a certain confinement enhancement factor, H_{ST}, which modifies the confinement time calculation based on the ST scaling assumption [9]. The controller module implements the user-supplied feedback control law at each transport time step to update the actuator requests based on the current ι-profile extracted from TRANSP, the reference actuator trajectory u_r, and the reference state trajectory ι_r. The boundary shape request module calculates the coil currents at each time step to best fit a prescribed plasma boundary shape.

For the simulations in this work, the target (or reference) state trajectory $\iota_r(\hat{\rho}, t)$ is generated through an open-loop TRANSP simulation based on arbitrarily selected actuator trajectories to ensure the target is feasible (i.e., it is a solution of the MDE). Both for control design and closed-loop simulations, the non-dimensional spatial domain ($\hat{\rho} \in [0,\ 1]$) is divided into $l = 21$ radial nodes, hence, the radial grid size is $\Delta\hat{\rho} = 0.05$.

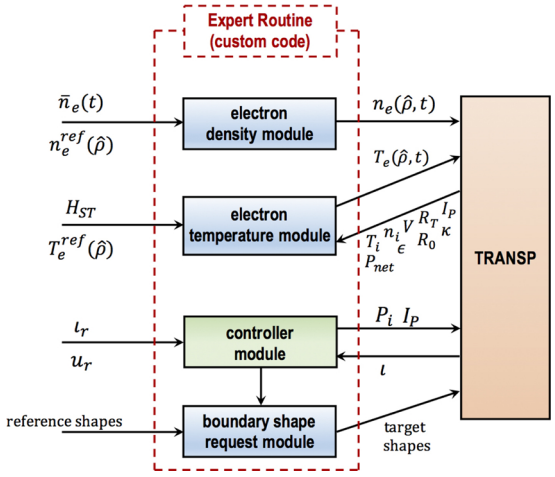

Fig. 2. Communication flow between TRANSP and the Expert routine [6].

4.1. Rejection of disturbed initial conditions and inputs

In this simulation, both initial-condition-perturbation and input-disturbance rejection capabilities are assessed by setting

$$u(t) = \begin{cases} u_r + u_d, & t < 1\,\mathrm{s} \\ \Delta u(t) + u_r + u_d, & t \geq 1\,\mathrm{s} \end{cases} \tag{16}$$

where u_d stands for the constant disturbance inputs (15% of the reference for the density and plasma current, 10% of the reference for the beam powers). The feedback controller is turned on at $t = 1$ s, and the simulation results are summarized in Fig. 3. The time evolution of the optimal physical inputs are illustrated in Fig. 3(a). The corresponding time evolution of the selected optimal outputs are depicted in Fig. 3(b) along with their respective targets. Fig. 3(c) compares actual and reference $\iota(\hat{\rho})$ profiles achieved at different instants in time. The difference between $\iota_r(t = 1)$ and $\iota(t = 1)$ in Fig. 3(c) is the consequence of introducing input perturbations for $t \in [0, 1]$ without feedback control. This difference can also be appreciated in Fig. 3(b). Despite this difference, the feedback controller is able to start tracking the reference profile after it is turned on at $t = 1$ s, showing almost perfect tracking after $t = 2.5$ s as shown in Fig. 3(b) and (c). The results of this simulation show that the proposed controller is capable of utilizing all physical actuators, including plasma density, to effectively regulate the ι-profile around a target profile in spite of the disturbances.

4.2. Rejection of changes in confinement

In this simulation study, the simultaneous tracking and disturbance-rejection capabilities of the controller are further tested by imposing a linear decrease in the confinement enhancement factor (H_{ST}) from 1.25 to 0.75 during $t \in [2.5,\ 5]$ s. This artificial decrease in the H_{ST} factor represents the possible confinement variations that might happen in NSTX-U experiments. Note that in addition to the variations in the H_{ST} factor, the same input disturbances as in (16) and initial-condition perturbations as in the previous simulation study are applied in this simulation. For simplicity, the line-averaged density is kept at its reference value, and only plasma current and neutral-beam powers are used as actuators for this simulation study. Simulation results are summarized in Fig. 4. Note from Fig. 4(b) that the outputs are once again effectively regulated around their desired values after the

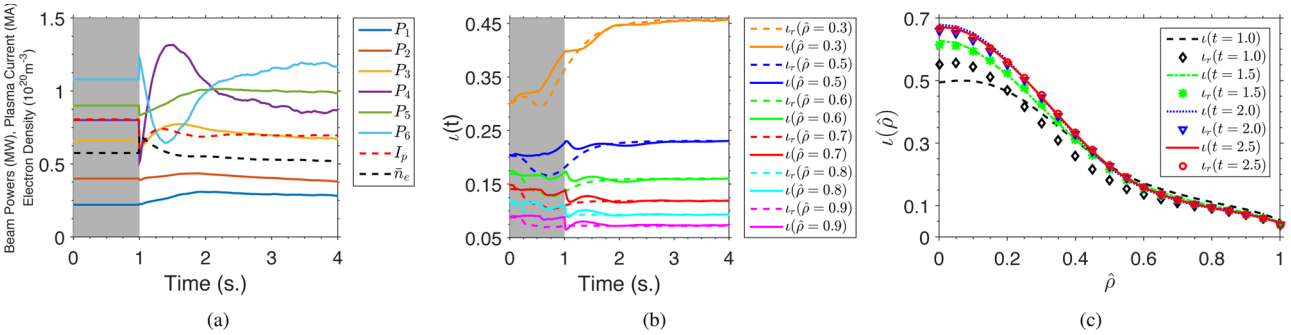

Fig. 3. Results of the tracking simulation against perturbed initial conditions and input disturbances (Section 4.1): (a) time evolution of the physical actuators, (b) time evolution of the select optimal outputs, and (c) target and achieved rotational transform profiles at select times. (The controller is off in the grey region.)

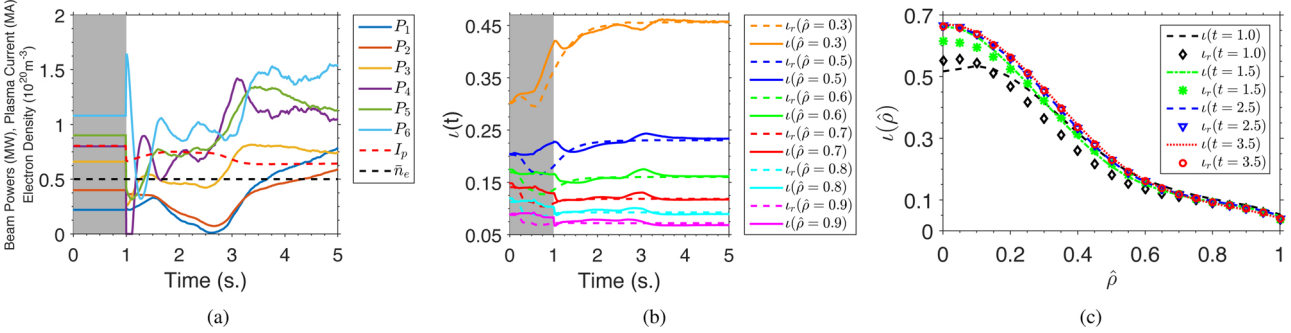

Fig. 4. Results of the tracking simulation against decreasing confinement factor (Section 4.2): (a) time evolution of the physical actuators, (b) time evolution of the select optimal outputs, and (c) target and achieved rotational transform profiles at select times. (The controller is off in the grey region.)

controller is turned on and before the confinement decrease is imposed at 2.5 s. This can also be noted from Fig. 4(c) by comparing the actual profile ι and the desired target profile ι_r at $t = 2.5$ s. Note also from Fig. 4(b) that the states suddenly deviate from their targets after $t = 2.5$ s, when the confinement decrease is imposed. The controller, however, quickly mitigates the effect of this sudden confinement change, providing once again almost excellent profile matching at $t = 3.5$ s as shown in Fig. 4(c). Based on this simulation analysis, the proposed controller is shown to be effective in regulating the ι-profile even if the confinement changes.

5. Conclusions and future work

In this work, an NSTX-U-tailored plasma response model is embedded into the control design process to synthesize a linear-quadratic-integral, optimal controller capable of regulating the rotational transform profile (or, equivalently, the current density profile), around a desired target profile. The performance of a current-profile controller under the presence of disturbances due to input/initial-condition perturbations and confinement factor changes is tested for the first time in closed-loop TRANSP simulations The contribution of this work resides equally on the control design and on the TRANSP-based closed-loop simulation for current-profile regulation. The promising tracking performance motivates the implementation of the proposed controller in NSTX-U once critical diagnostics and actuators are commissioned and plasma operation resumes.

Acknowledgment

Work supported by the US DoE (DE-AC02-09CH11466).

References

[1] J. Menard, et al., Overview of NSTX Upgrade initial results and modelling highlights, Nucl. Fusion 57 (10) (2017) 102006.
[2] S.P. Gerhardt, et al., Exploration of the equilibrium operating space for NSTX-Upgrade, Nucl. Fusion 52 (8) (2012) 083020.
[3] NSTX Upgrade Five Year Plan, (2018) https://nstx.pppl.gov/.
[4] Z. Ilhan, et al., Physics-based control-oriented modeling of the current density profile evolution in NSTX-Upgrade, Fusion Eng. Des. 123 (2017) 564–568.
[5] TRANSP Homepage, (2015) http://w3.pppl.gov/transp/.
[6] M. Boyer, et al., Central safety factor and β_N control on NSTX-U via beam power and plasma boundary shape modification, using TRANSP for closed loop simulations, Nucl. Fusion 55 (5) (2015) 053033.
[7] J. Wesson, Tokamaks, Clarendon Press, Oxford, UK, 1984.
[8] D.S. Naidu, Optimal Control Systems, CRC Press, 2002.
[9] S. Kaye, et al., Energy confinement scaling in the low aspect ratio National Spherical Torus Experiment (NSTX), Nucl. Fusion 46 (10) (2006) 848.